

A MAGNETOHYDRODYNAMIC MODEL OF THE M87 JET. II. SELF-CONSISTENT QUAD-SHOCK JET MODEL FOR OPTICAL RELATIVISTIC MOTIONS AND PARTICLE ACCELERATION

MASANORI NAKAMURA¹ & DAVID L. MEIER²

¹Institute of Astronomy & Astrophysics, Academia Sinica, 11F of Astronomy-Mathematics Building, AS/NTU No. 1, Taipei 10617, Taiwan; nakamura@asiaa.sinica.edu.tw and

²Jet Propulsion Laboratory, California Institute of Technology, Pasadena, CA 91109, USA; david.l.meier@jpl.nasa.gov

Draft Version, Accepted for publication in ApJ

ABSTRACT

We describe a new paradigm for understanding both relativistic motions and particle acceleration in the M87 jet: a magnetically dominated relativistic flow that naturally produces four relativistic magnetohydrodynamic (MHD) shocks (forward/reverse fast and slow modes). We apply this model to a set of optical super- and subluminal motions discovered by Biretta and coworkers with the *Hubble Space Telescope* during 1994 – 1998. The model concept consists of ejection of a *single* relativistic Poynting jet, which possesses a coherent helical (poloidal + toroidal) magnetic component, at the remarkably flaring point HST-1. We are able to reproduce quantitatively proper motions of components seen in the *optical* observations of HST-1 with the same model we used previously to describe similar features in radio VLBI observations in 2005 – 2006. This indicates that the quad relativistic MHD shock model can be applied generally to recurring pairs of super/subluminal knots ejected from the upstream edge of the HST-1 complex as observed from radio to optical wavelengths, with forward/reverse fast-mode MHD shocks then responsible for observed moving features. Moreover, we identify such intrinsic properties as the shock compression ratio, degree of magnetization, and magnetic obliquity and show that they are suitable to mediate diffusive shock acceleration of relativistic particles via the first-order Fermi process. We suggest that relativistic MHD shocks in Poynting-flux dominated helical jets may play a role in explaining observed emission and proper motions in many AGNs.

Subject headings: galaxies: individual: M87 — galaxies: active — galaxies: jets — methods: numerical — MHD

1. INTRODUCTION

In this paper we apply our previous relativistic MHD shock model for the 2005 M87 radio jet (Nakamura *et al.* 2010, hereafter Paper I) to the *optical* super/subluminal knots discovered by Biretta *et al.* (1999) using the *Hubble Space Telescope* (HST) at five epochs between 1994 and 1998. These observations reveal superluminal features in the range $5c - 6c$ with some subluminal components located around $0''.8 - 1.6''$ (projected) from the core (or $\sim 260 - 520$ pc de-projected for a viewing angle of $\sim 14^\circ$; Wang & Zhou 2009). This region has been named as the “HST-1” complex. So far HST-1 is one of the most energetic elements of the M87 jet, exhibiting both fast and slow (super/subluminal) motions as well as the birth of new components and the fading of older ones (Biretta *et al.* 1999; Cheung *et al.* 2007). The global structure of the jet is characterized as a parabolic stream on the sub-arcsecond scale, which changes into a conical stream beyond one arcsecond; HST-1 is indeed the narrow “neck” in the jet, indicating an over-collimated focal point (or “recollimation shock”) (Asada & Nakamura 2012; Nakamura & Asada 2013).

Multi-band light curves of HST-1 reveal an impulsive flare event that had a peak in 2005 (Harris *et al.* 2006; Cheung *et al.* 2007; Madrid 2009). As reported in Cheung *et al.* (2007), between 2005 December and 2006 February, the component HST-1c, which had been ejected during 2004 – 2005 from HST-1d (the upstream edge in the HST-1 complex), *split into two bright features*: a faster moving component (c1: $4.3c \pm 0.7c$) and a slower moving one (c2: $0.47c \pm 0.39c$). The ejection of these components is believed to be associated with the HST-1 flare occurring in 2005. The simultaneous rise and fall of light curves at all wavelengths

(radio, optical, NUV, and X-ray bands) indicate that the flare was a local event caused by a simple compression at HST-1 (Harris *et al.* 2006, 2009), which created an increase of the synchrotron particle energy at all wavelengths equally and a fractional polarization in the optical band at a level from 20% to 40% (Perlman *et al.* 2011).

Furthermore, the very high energy (VHE) γ -ray emission in the TeV band that occurred in 2005 (Aharonian *et al.* 2006) may be associated with contemporaneous radio-to-X-ray flaring of HST-1, while the nucleus itself was in a *quiescent* phase from radio to X-ray bands during the γ -ray flare event (Abramowski *et al.* 2012). The VLBA monitoring at 22/43 GHz of EGRET blazars has established a statistical association that γ -ray flares at high levels occur shortly after ejections of new superluminal components of parsec-scale jets in nearby VLBI cores (Jorstad *et al.* 2001). Thus, we suggest that the VHE flare associated with the superluminal knot ejection in M87 is intrinsically similar to events seen in other blazars.

Paper I proposed a model to explain the ejected super/subluminal VLBA knots from HST-1d in 2005 – 2006 (Cheung *et al.* 2007) as a pair of forward/reverse fast-mode MHD shocks in a strongly magnetized relativistic flow that possesses an ordered helical field component. A simple test of this model would be to find another appropriate candidate quad shock complex in the M87 jet. Here, we seek it in the earlier HST observations of 1994 – 1998 (Biretta *et al.* 1999), and we suggest that HST-1e ($6.00c \pm 0.48c$) / HST-1 East ($0.84c \pm 0.11c$) in their observations are a similar pair to HST-1c2/c1. With several moderate changes in model parameters, we then reproduce the component motions with our quad MHD shock model and show that the shock conditions

there are ideal for particle acceleration. This paper is organized as follows. In §2, we outline the numerical model. In §3, we describe our numerical results. Discussions and conclusions are given in §4.

2. NUMERICAL AND PHYSICAL MODEL

2.1. Component Geometry and Emission

A detailed description of our model concept (*a magnetically dominated relativistic flow*) is in §2 of Paper I. Using a linear scale of $78 \text{ pc arcsec}^{-1}$ ($D = 16 \text{ Mpc}$; Tonry 1991), a proper motion of 1 mas yr^{-1} at M87 corresponds to an apparent velocity of $0.25c$. In Biretta *et al.* (1999), it is suggested that the most upstream component of the HST-1 complex (HST-1 East, at 870 mas from the core and moving relatively slowly at $0.84c \pm 0.11c$) had given birth to at least three superluminal components. In 1995, HST-1 East appeared to eject a new component at 870 mas from the core (HST-1e: $6.00c \pm 0.48c$).

However, we suggest a different scenario based on the later observations of Cheung *et al.* (2007). In their VLBA observations, HST-1d is the dominant feature in the HST-1 complex in the early epochs before 2005. Between 2005 and 2006, the location of HST-1d is basically *stationary* to within $\sim 2 \text{ mas}$ (i.e., its motion is $< 0.25c$) at 860 mas from the core. Then, the radio knot HST-1c must have *emerged from* HST-1d in the downstream direction ($> 860 \text{ mas}$). Since the upstream region of the HST-1 complex seems to be well resolved in VLBA (but not so well resolved in HST) observations, we thus consider HST-1 East to be a moving component ejected from the stationary HST-1d (the upstream edge in the HST-1 complex).

Following Paper I, we assert that the lateral gas compression at HST-1 (and its expansion after maximum squeezing) causes the ejection of new shock components. Very recently, Liu *et al.* (2013) suggested the de Laval nozzle-like shape as an explanation for the multi-wavelength light curves during the 2005 flaring event at HST-1 described above; an adiabatic compression/expansion of the flow cross section may be responsible for observed multi-wavelength synchrotron light curves (e.g., Harris *et al.* 2006, 2009). Also, as we have described in Paper I, axisymmetric non-relativistic and relativistic MHD numerical simulations of strongly magnetized, super-fast magnetosonic flows with a helically twisted magnetic field component produce a magnetic chamber, which opens and closes intermittently, ejecting multiple quad shock components into the downstream “Nose Cone” region (Lind *et al.* 1989; Komissarov 1999).

During the past few decades, an extensive monitoring of the M87 jet downstream from HST-1 ($1 - 18''$ or $0.1 - 1.5 \text{ kpc}$ in projection) has been conducted in a wide range of wavelengths at radio (VLA), optical (HST), and X-ray (Chandra) bands. Emissions from radio to X-ray bands resemble each other in morphology, indicating a common synchrotron radiation process (Marshall *et al.* 2002; Wilson & Yang 2002; Perlman & Wilson 2005). The observations also suggest that *in situ* particle acceleration at shocks (via the first-order Fermi process; Blandford & Ostriker 1978) occurs in the large scale M87 jet, as evidenced both from the electron lifetime scale (much shorter than the jet travel time from the nucleus) and from spectral fits to the broadband spectra. A relativistic particle energy distribution $n(E)dE \propto E^{-\delta}dE$ would need a spectral index steeper than $\delta = 2$ in order to produce the radio through optical to X-ray synchrotron spectrum in the M87 jet (at HST-1 and its downstream region); synchrotron

models have been fit with $\delta = 2.2$ at all energies and all locations along the jet (Perlman & Wilson 2005) and with about $\delta = 2.36$ on average (Liu & Shen 2007). These agree very well with the conditions needed for diffusive shock acceleration (DSA) [$\delta = 2 - 2.5$; e.g., Kirk & Dendy (2001); Rieger *et al.* (2007); Schure *et al.* (2012)].

Intensity profiles, which are taken across the jet (FWHM) at knot A for HST and VLA observations, yield motions of $1''.13$ in the radio band and only $0''.85$ in the optical (Sparks *et al.* 1996). Note that average intensity profiles normal to the jet axis for knots D, E, F, I, B, and C also have a similar tendency; optical knots are more compact and centrally concentrated than the radio knots. Comparison between the optical and radio polarimetry by Perlman *et al.* (1999) provides additional evidence that optical- and radio-emitting electrons are not completely co-located. Their results show that the degree of polarization varies less in the radio than in the optical, indicating that the optical-emitting electrons are located closer to the jet axis, whereas most of the radio-emitting electrons are located nearer the jet surface.

2.2. Numerical Setup

The basic numerical treatment is essentially the same as in Paper I (see, §3 and 4). We solve the special relativistic MHD (SRMHD) equations in a cylindrical 1.5-dimensional approximation (axisymmetry in the azimuthal direction ϕ) along the z -axis at a fixed cylindrical radius r . Our normalization details are summarized in Table 1. Compared to Paper I for modeling HST-1c2/c1 (Cheung *et al.* 2007), here we consider several moderate changes regarding the initial conditions for modeling HST-1e/East (Biretta *et al.* 1999). By assuming a viewing angle $\theta_v \sim 14^\circ$ at HST-1 (Wang & Zhou 2009), a maximum “intrinsic” speed (including an error) in HST observations of the M87 jet can be estimated from the “apparent” speed of the fastest moving component HST-1e: $\beta_{\text{app}} = 6.00 \pm 0.48$ (Biretta *et al.* 1999) with $\beta_{\text{int}} = \beta_{\text{app}} / (\beta_{\text{app}} \cos \theta_v + \sin \theta_v) \simeq 0.992$, where $\beta \equiv V/c$. It is assumed that the intrinsic speed is associated with the jet fluid speed $\beta_H = V_H/c$, with $\beta_{\text{int}} \lesssim \beta_H$ (Biretta *et al.* 1995)¹.

We model the jet as a highly magnetized medium with low plasma- β values (a ratio of the gas pressure to the magnetic pressure) $\beta_p < 0.1$ and small magnetic obliquity angles $\sim 10^\circ$ (measured in the rest frame of the fluid). The jet is injected as a trans-fast magnetosonic, relativistic flow (Lorentz factor: $\gamma \simeq 11.48$) into a medium flowing with a sub-relativistic speed ($\gamma \simeq 1.07$). Under these conditions, the jet naturally produces a set of four relativistic MHD shocks in the system. The computational domain $z \in [-0.04, 2.0]$ (parsec in a dimensional scale), which is resolved with 5100 grid points, assigns two uniform states (up: upstream and down: downstream) separated at $z = 0.0$. Time integration is followed until $t = 2.0$ ($\sim 6.4 \text{ yr}$) to examine an early phase of relativistic MHD shock propagation and inspect the individual wave fronts.

The following initial conditions are prescribed:

$$(\rho, V_\phi, V_z, B_\phi, B_z, p)^{\text{up}} = (1.0, 0, 0.996, 8.0, 3.0, 0.405)$$

on the upstream side ($-0.04 \leq z \leq 0.0$) and

$$(\rho, V_\phi, V_z, B_\phi, B_z, p)^{\text{down}} = (1.0, 0, 0.360, 0.7, 3.0, 0.052)$$

¹ Readers can refer to the related argument in section 2 of Nakamura & Asada (2013) concerning the possibility that the observed proper motions are correlated with the underlying bulk flow in AGN jets.

on the downstream side. (The numerical time integration uses a CFL number of 0.5.) The main difference between initial conditions in the present paper and in Paper I is the implementation of *two* uniform states of B_ϕ on each side (measured in the rest frame of the galaxy), while Paper I specifies one uniform state on both sides. This treatment will affect mainly the compression ratio r_{cmp} at the forward fast-mode shock (as is discussed in §5 of Paper I). Note that $B_\phi^{\text{up}}/B_\phi^{\text{down}} \simeq 1.07$ (quasi-uniform state on both sides) in current initial conditions, if we measure in the rest frame of the fluid.

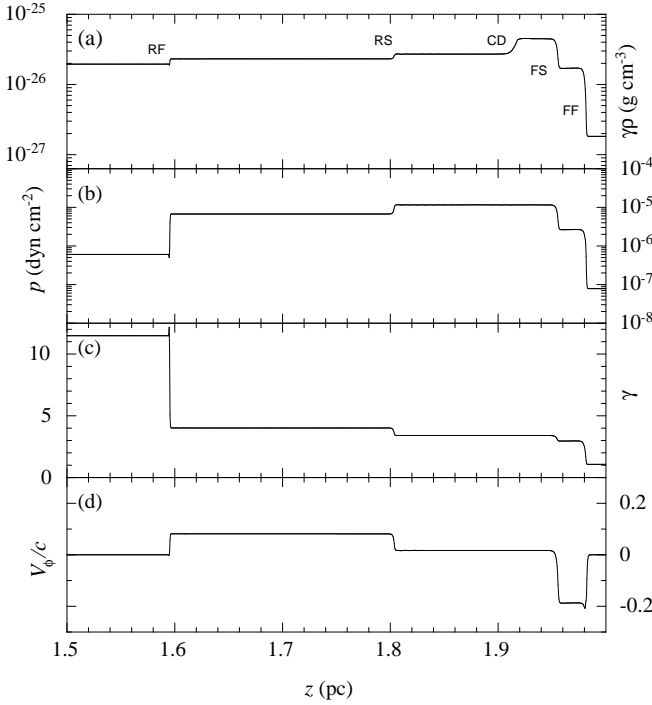


FIG. 1.— (a) – (d) $\log(\gamma\rho)$, $\log(p)$, γ , and V_ϕ/c , respectively, shown at $t = 2.0$. Only the region $1.5 \leq z \leq 2.0$ is displayed. Note that panels (a) – (d) are measured in the rest frame of the galaxy. Each discontinuity is labeled in (a).

3. NUMERICAL AND PHYSICAL RESULTS

3.1. Jet Flow and Shock Propagation

Figure 1 shows the propagation of the relativistic MHD wave fronts; snapshots of various quantities at $t = 2.0$ are illustrated in the rest frame of the galaxy. The distribution of proper density $\gamma\rho$ shows the quad MHD shock pattern plus a contact discontinuity (CD or entropy wave), all with constant speeds. While all features move downstream in the galaxy frame, in a reference frame that co-moves with the jet plasma near the CD, these waves propagate in both the forward (F) and reverse (R) directions. Here we adopt the convention of counting shocks beginning with the one farthest from the origin of the disturbances (HST-1). Two of the four shocks, the first and the fourth, are forward fast-mode (FF) and reverse fast-mode (RF) shocks, respectively. The other two, the second and the third, are forward slow-mode (FS) and reverse slow-mode (RS) shocks.

Basic features shown in Fig. 1 are similar to those in Fig. 3 of Paper I. The flowing gas is compressed twice across the first

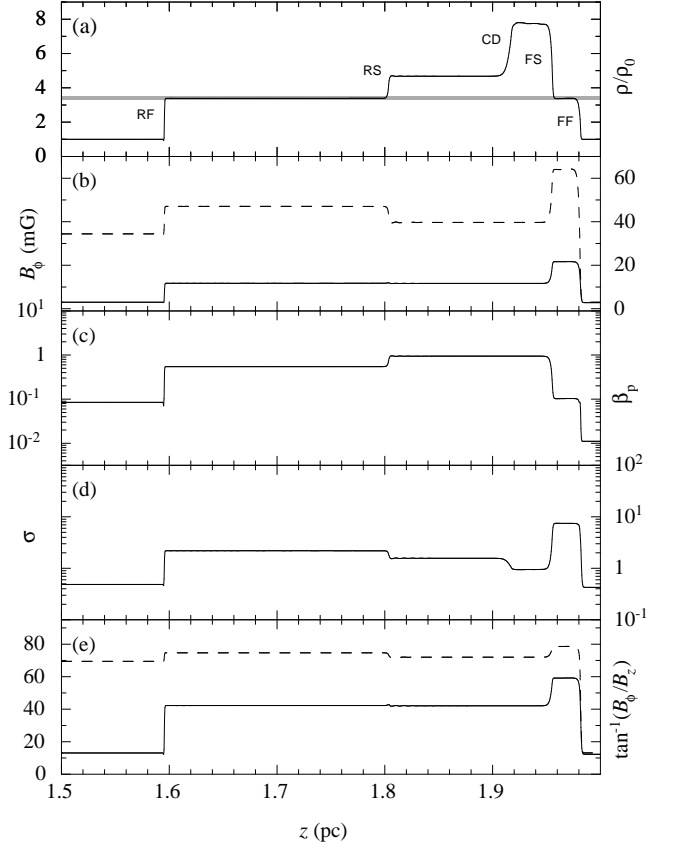


FIG. 2.— (a) – (e) ρ/ρ_0 , B_ϕ , $\log(\beta_p)$ (plasma- β), $\log(\sigma)$ (magnetization parameter), and θ (magnetic obliquity angle), respectively, shown at $t = 2.0$. Only the region $1.5 \leq z \leq 2.0$ is displayed. Note that all quantities in each panel are measured in the rest frame of the fluid (drawn as a solid line), with the exception of the broken lines in (b) and (e), which are measured in the rest frame of the galaxy. Each discontinuity is labeled in (a). A gray shaded area in (a) indicates a proper compression ratio ($r_{\text{cmp}} \sim 3.3\text{--}3.5$) for a relativistic DSA.

(FF) and second (FS) shocks, while it is expanded in crossing the third (RS) and last (RF) shocks respectively, as seen in (a) and (b). As a result, the gas pressure at the accumulated region between FS and RS shocks (RS-CD-FS) increases by almost two orders of magnitude compared to the pre-shocked region by twice compressions at the FF and FS shocks. As one moves from large to small z , γ increases with gradual steps in the first, second, and third shocks, and greatly increases in the last shock to the injection level $\gamma \simeq 11.48$ shown in (c). From (d), V_ϕ changes as well at each shock discontinuity; the region FF-FS and the region RS-RF are *counter-rotating* when viewed from a frame that rotates with the plasma near the CD, as was also seen in Paper I.

Strengths and propagation speeds of the four shocks remain constant with distance as they propagate in our coordinate system: axial propagation (z -direction) in a uniform medium (constant sound and Alfvén speeds) in a fixed-radius cylindrical shell. Individual speeds of shock fronts are estimated as $V_{\text{FF}} \sim 0.99c$, $V_{\text{FS}} \sim 0.98c$, $V_{\text{RS}} \sim 0.90c$, and $V_{\text{RF}} \sim 0.80c$, respectively. For a viewing angle of $\theta \sim 14^\circ$ at HST-1 (Wang & Zhou 2009), the faster component HST-1 ϵ has $\sim 0.99c$, while the slower component HST-1 East has $\sim 0.79c$. As is mentioned in Paper I, a separation of observed super/subluminal components can be identified as distinct proper motions of two fast-mode MHD shocks (FF/RF),

instead of two slow-mode MHD shocks due to an ineffectiveness of the DSA in slow-mode shocks (e.g., Kirk & Duffy 1999). Thus, our numerical model is consistent with observations (Biretta *et al.* 1999).

3.2. Particle Acceleration

In order to examine the efficiency of high energy particle acceleration by the DSA, *i.e.* the first-order Fermi process (Blandford & Ostriker 1978), we show several quantities in Fig. 2 that are measured in the rest frame of the fluid. Panel (a) shows the shock compression ratio r_{cmp} of the density ρ to the ambient value ρ_0 . This ratio at each shock front is ~ 3.4 at both the FF and RF, ~ 2.3 at the FS, and ~ 1.4 at the RS.

For the DSA process in non-relativistic shocks (shock propagation speed $V_s \ll c$), the spectral slope δ in a power-law distribution of the relativistic particle energy does not depend on the details of the flow (the magnetic field orientation near the shock, the mechanism of particle diffusion, or other microscopic physics involved). Instead, δ depends only on the compression ratio r_{cmp} (e.g., Bell 1978) as

$$\delta \equiv \frac{r_{\text{cmp}} + 2}{r_{\text{cmp}} - 1}, \quad (1)$$

where $\delta \simeq 2$ corresponds to strong shocks with a maximum compression ($r_{\text{cmp}} \simeq 4$) (Drury 1983; Blandford & Eichler 1987).

However, in the case of relativistic shocks ($V_s \sim c$), $\delta \sim 2.2$ – 2.3 is expected (Waxman 1997; Bednarz & Ostrowski 1998; Kirk *et al.* 2000; Achterberg *et al.* 2001), corresponding to $r_{\text{cmp}} \sim 3.3$ – 3.5 . So, our numerical result of $r_{\text{cmp}} \sim 3.4$ at the FF/RF is entirely consistent with the expected value for relativistic DSA theory and observations (Perlman & Wilson 2005; Liu & Shen 2007). Note that an efficiency of the particle acceleration by the relativistic DSA crucially depends on background conditions, such as both the magnetization and magnetic obliquity of the upstream plasma. Furthermore, $\delta \sim 2.2$ – 2.3 may be valid only in quasi-parallel (small magnetic obliquity) shocks, while a large departure from this range is confirmed in Monte Carlo simulations (e.g., Bednarz & Ostrowski 1998; Niemiec & Ostrowski 2006).

Panel (b) of Fig. 2 shows the distribution of B_ϕ in the rest frame of the fluid as well as the galaxy. It increases across the first shock, decreases across the second one, increases again across the third shock, and finally decreases across the fourth one. In the rest frame of the galaxy, the azimuthal field component is much larger than the axial field component ~ 10 mG, while in the rest frame of the fluid both are comparable. A field of ~ 10 mG near the HST-1 complex has been derived from variability time scales in optical and X-ray observations (Perlman *et al.* 2003). From panel (c) of Fig. 2, we find the gas pressure near the CD is in approximate equipartition with the magnetic pressure in the rest frame of the fluid ($\beta_p \sim 1$, as was also seen in Paper I).

Using the definition in Narayan *et al.* (2011), the magnetization parameter σ in the local plasma rest frame is defined as the ratio of the Poynting flux to the matter energy flux:

$$\sigma \equiv \frac{B_\phi^2}{4\pi\gamma^2\rho c^2}. \quad (2)$$

We also define the obliquity angle θ in the local plasma rest frame:

$$\theta \equiv \tan^{-1} \left(\frac{B_\phi}{\gamma B_z} \right). \quad (3)$$

Recent 2.5D/3D particle-in-cell simulations (e.g., Spitkovsky 2008; Sironi & Spitkovsky 2009) confirm that particle acceleration is mostly mediated by the DSA process for quasi-parallel field ($\theta \lesssim 10^\circ$), but shock drift acceleration (SDA) is the main acceleration mechanism for larger, yet still *subluminal* (in *de Hoffmann-Teller* frame: *de Hoffmann & Teller* 1950) magnetic obliquity. The critical angle for the shock to be “subluminal”² decreases with increasing upstream bulk Lorentz factor γ and magnetization σ but stays confined within a relatively narrow range ($\theta_{\text{crit}} \simeq 26^\circ$ – 42°) for moderate magnetization ($\sigma \lesssim 1.0$) (Sironi & Spitkovsky 2009). Panel (d) and (e) of Fig. 2 show the distribution of σ in the rest frame of the fluid and θ in both the fluid rest and galaxy frames. We can see $\sigma \lesssim 0.5$ and $\theta \lesssim 13^\circ$ upstream of both the FF and RF, indicating the DSA process may be feasible in both quasi-parallel shocks FF/RF.

In our model, the quad shock system is initiated at HST-1 and propagates in a conical streamline. As is shown in Paper I, B_ϕ becomes much more dominant than B_z in the downstream direction. Furthermore, study of proper motions indicate a systematic deceleration of propagating knots (Biretta *et al.* 1995, 1999; Meyer *et al.* 2013). By combining these aspects, θ eventually becomes large, indicating a quasi-perpendicular shock. In order to maintain a universal value $\delta \sim 2.2$ – 2.3 for the relativistic DSA, large amplitude MHD turbulence ($\kappa_\perp/\kappa_\parallel \simeq 1$, where κ_\perp and κ_\parallel are the cross-field and the parallel diffusion coefficient, respectively) near the shock would be required (*otherwise*, δ can be much steeper than the above asymptotic values in the absence of large turbulence, e.g., Bednarz & Ostrowski 1998; Ostrowski & Bednarz 2002; Niemiec & Ostrowski 2004; Niemiec *et al.* 2006). Note that κ_\perp and κ_\parallel are in units of cr_g , where r_g is the particle gyration radius in the unperturbed background field. Therefore, it may be beyond our scope, but recent relativistic MHD simulations of mildly relativistic shocks with $V_s \sim 0.4c$ – $0.9c$ suggest that perpendicular shocks produce highly turbulent field amplification in the postshock region (Mizuno *et al.* 2011).

Finally we remark on the efficiency of shock dissipation in highly magnetized (Poynting-flux dominated) relativistic flows. Komissarov (2012) found that the dissipation efficiency (ratio of thermal to total energy flux densities) of a fast magnetosonic shock is still a quite high fraction, $\sim 30\%$ ($\sigma = 1.0$)– 80% ($\sigma = 0.1$) of the total energy flux. This is the case mainly because only the kinetic energy is dissipated, and it represents only a small fraction of the total energy flowing through the shock. We therefore propose that our quad relativistic shock model may explain not only the relativistic bulk motions in a pair of super/subluminal features in AGN jets, but also the particle acceleration that takes place in them.

4. DISCUSSION AND CONCLUSIONS

The basic assumption of our model posits ejection of a *single* relativistic jet, which naturally produces four MHD shocks, from a stationary feature (standing over-collimation Mach disk / oblique shock system) in compact radio sources that produce a pair of super/subluminal knots. In M87, we believe that the HST-1 complex is the place where these events occur (Biretta *et al.* 1999; Cheung *et al.* 2007). Very recently, Giroletti *et al.* (2012) reported two superluminal com-

² If the shock is “superluminal”, it is difficult to for the DSA process to proceed (Begelman & Kirk 1990).

ponents ejected from HST-1 after 2007 (component 2 in 2008 and component 3 in 2010). In their analysis, component 2 is identified as being similar to HST-1c (seen in Cheung *et al.* (2007)); it eventually splits into two sub-components, although the authors argue that the slow sub-component may be an underlying, standing or very slowly moving feature (a detailed proper motion analysis was not conducted for this sub-component). *However*, we suggest that component 2 may represent the ejection of a third quad relativistic shock system in the M87 jet, which possesses both sub- (reverse) and superluminal (forward) features. Giroletti *et al.* (2012) also pointed out simultaneous timings between the superluminal component ejections and VHE flares in 2008 and 2010 (Abramowski *et al.* 2012), suggesting that structural changes at the upstream edge of HST-1 are related to these flares.

Very recently, Meyer *et al.* (2013) studied proper motions of the M87 jet on arcsecond (kiloparsec) scales by using more than a decade of *HST* archival imaging. Significant new apparent motions $\gtrsim c$ have been found at the knot A/B/C complex. Furthermore, knots C and A move in opposite directions *transverse* to the jet axis with $V \gtrsim 0.1c$ in projection. This may indicate a counter-rotational motion around the jet axis as expected for a pair of fast-mode shocks (FF/RF) in an older (and now much larger) quad MHD shock system. (Such motions occur in our current simulation of the much smaller HST-1 complex, as seen in (d) of Fig. 1 and also in Paper I.) Overall velocity profiles along the jet axis, as well as transverse to that axis, may be explained as embedded flow trajectories within systematic helical magnetic fields (Meyer *et al.* 2013). Velocity components that lie upstream of knot A are observed to still have highly relativistic, and thus one-sided (i.e., *negative*), transverse motions (Doppler boosted towards us). Once the jet becomes mildly relativistic, however, we are able to track the full (i.e., both *positive* and *negative*) transverse motions of the helical pattern in projection. Furthermore, there is a conspicuous “tip-to-tail” alignment of almost all the velocity vectors within the knot A/B/C complex, strongly suggesting a flattened view of a helical motion which might result in such a “zig-zag” pattern. In the framework of a quad MHD shock system, a pair of fast-mode shocks (FF/RF), corresponding to the knots C/A, may be responsible for driving the helical distortion near the postshock region of B via the current-driven helical kink ($m = 1$) instability (Nakamura & Meier 2004). Thus, we propose that the region A/B/C may be a good example (on the kiloparsec scale) of the interplay between the MHD shocks and current-driven instability, where the magnetic field plays a fundamental role in the M87 jet dynamics, as originally suggested in Paper I.

It is widely believed that moving shocks in jets (“shock-in-jet” model) are responsible for the synchrotron emission in blazars (e.g., Blandford & Königl 1979; Marscher 1980). A subset of the preceding, superluminal (forward shock) and the following, stationary/subluminal (reverse shock) features are

frequently seen in VLBI observations (Jorstad *et al.* 2005; Lister *et al.* 2009). Among shock-in-jet models, the following two major scenarios have been discussed in a non-MHD framework: (1) a collision of the faster shock with either the preceding slowly moving shock (“internal shock” model: e.g., Spada *et al.* 2001) or (2) a standing shock complex (e.g., Daly & Marscher 1988; Sokolov *et al.* 2004). Note that both forward and reverse sonic shocks are expected in these models. An extension of the internal shock model with a perpendicular MHD forward/reverse shocks has been performed by Mimica *et al.* (2007). As mentioned in §1, strong γ -ray flares occur after ejections of new superluminal components from parsec-scale regions of jets in nearby VLBI cores (Jorstad *et al.* 2001). Instead of an internal shock scenario, we suggest here that there is a *standing* shock at HST-1 based on the observational aspects. Furthermore, because of the strong polarization associated with the knots in M87, as well as the superluminal motion, we must model these shocks using special relativistic magnetohydrodynamic simulations.

In this paper, we investigate a pair of super/subluminal motions in the M87 jet based on the quad relativistic MHD shock model (Nakamura *et al.* 2010). The model concept consists of ejection at HST-1 of a *single* relativistic Poynting jet, which possesses a coherent helical (poloidal + toroidal) magnetic component that naturally produces such features, as a counterpart to the hydrodynamic Mach disk - oblique shock system. HST-1e/East, which were identified in HST observations (Biretta *et al.* 1999), are modeled quantitatively with one-dimensional axisymmetric SRMHD simulations. We conclude that forward/reverse fast-mode MHD shocks are a promising explanation for the observed features, not only with regard to their intrinsic motions, but also in the efficiency of the diffusive shock acceleration (through the first-order Fermi process) of non-thermal particle accelerations at the shock fronts. Three fundamentals at the fast-mode MHD shocks derived from the simulations (shock compression ratio, degree of magnetization, and magnetic obliquity (magnetic pitch angle)) are suitable to mediate a Fermi-I process.

While we do not yet fully investigate the hypothesis that “all relativistic jets are dominated by the toroidal magnetic field component in the observer’s frame”, $B_\phi/B_z \sim \gamma$ (Lyutikov *et al.* 2005) certainly holds in the interknot (inter-shock) region of the M87 jet as we found ($B_\phi/\gamma/B_z \sim 1$ in the fluid frame). Therefore, we suggest our model may be applicable to many super/subluminal features of AGN jets in general.

M.N. acknowledges part of this research was carried out under supported by the Allan C. Davis fellowship jointly awarded by the Department of Physics and Astronomy at Johns Hopkins University and the Space Telescope Science Institute. Part of this research also was carried out at the Jet Propulsion Laboratory, California Institute of Technology, under contract with the National Aeronautics and Space Administration.

REFERENCES

- Abramowski, A., *et al.* 2012, ApJ, 746, 151
 Achterberg, A., Blandford, R. D., & Goldreich, P. 1983, Nature, 304, 1983
 Achterberg, A., Gallant, Y. A., Kirk, J. G., & Guthmann, A. W. 2001, MNRAS, 328, 393
 Aharonian, F., *et al.* 2006, Science, 314, 1424
 Asada, K., & Nakamura, M., 2012, ApJ, 745, L28 (AN12)
 Bednarz, J., & Ostrowski, M. 1998, Phys. Rev. Lett., 80, 3911
 Begelman, M. C., & Kirk, J. G. 1990, ApJ, 353, 66
 Bell, A. R. 1978, MNRAS, 182, 147
 Biretta, J. A., Zhou, F., & Owen, F. N. 1995, ApJ, 447, 582
 Biretta, J. A., Sparks, W. B., & Macchetto, F. 1999, ApJ, 520, 621
 Blandford, R. D., & Königl, A. 1979, ApJ, 232, 34
 Blandford, R. D., & Eichler, D. 1987, Phys. Rep. 154, 1
 Blandford, R. D., & Ostriker, J. P. 1978, ApJ, 221, L29
 Cheung, C. C., Harris, D. E., & Stawarz, L. 2007, ApJ, 663, L65
 Daly, R. A., & Marscher, A. P. 1988, ApJ, 334, 539
 de Hoffmann, F., & Teller, E. 1950, Phys. Rev., 80, 692
 Drury, L.O’C. 1983, Rep. Prog. Phys. 46, 973

TABLE 1
UNITS OF PHYSICAL QUANTITIES FOR NORMALIZATION.

Physical Quantities	Description	Normalization Units	Typical Values
z	Length	L_0	3.1×10^{18} cm (1 parsec)
\mathbf{V}	Velocity field	c	3.0×10^{10} cm s $^{-1}$
t	Time	L_0/c	1.0×10^8 s (3.2 yr)
ρ	Density	ρ_0	1.7×10^{-27} g cm $^{-3}$
p	Pressure	$\rho_0 c^2$	1.5×10^{-6} dyn cm $^{-2}$
\mathbf{B}	Magnetic field	$\sqrt{4\pi\rho_0 c^2}$	4.3×10^{-3} G

- Gebhardt, K., Adams, J., Richstone, D., *et al.* 2011, ApJ, 729, 119
 Giroletti, M., *et al.* 2012, ARA&A, 538, L10 & Wilson, A. S. 2003, ApJ, 586L, L41
 Harris, D. E., Cheung, C. C., Biretta, J. A., Sparks, W. B., Junor, W., Perlman, E. S., & Wilson, A. S. 2006, ApJ, 640, 211
 Harris, D. E., Cheung, C. C., Stawarz, L., Biretta, J. A., & Perlman, E. S. 2009, ApJ, 699, 305
 Jorstad, S. G., *et al.* 2001, ApJ, 556, 738
 Jorstad, S. G., *et al.* 2005, AJ, 130, 1418
 Kirk, J. G., Guthmann, A. W., Gallant, Y. A., & Achterberg, A. 2000, ApJ, 542, 235
 Kirk, J. G., & Dendy, R. O. 2001, J. Phys. G, 27, 1589
 Kirk, J. G., & Duffy, P. 1999, J. Phys. G, 25, 163
 Kirk, J. G. (2004), Phys. Rev. Lett. 2004, 92, 1101
 Komissarov, S. S. 1999, MNRAS, 308, 1069
 Komissarov, S. S. 2012, MNRAS, 422, 326
 Langdon, A. B., Arons, J., & Max, C. E. 1988, Phys. Rev. Lett., 61, 779
 Lind, K. R., Payne, D. G., Meier, D. L., & Blandford, R. D. 1989, ApJ, 344, 89
 Lister, M., *et al.* 2009, AJ, 138, 1874
 Liu, W.-P., & Shen, Z.-Q. 2007, ApJ, 668, L23
 Liu, W.-P., Zhao, G.-Y., Chen, Y. J., Wang, C.-C., & Shen, Z.-Q. 2013, AJ, 146, 155L
 Lyutikov, M., Pariev, V. I., & Gabuzda, D. C. 2005, MNRAS, 360, 869
 Madrid, J. P. 2009, AJ, 137, 3864
 Marscher, A. P. 1980, ApJ, 235, 386
 Marshall, H. L., *et al.* 2002, ApJ, 564, 683
 Meyer E. T., Sparks W. B., Biretta J. A., Anderson J., Sohn S. T., van der Marel R. P., Norman C., Nakamura M. 2013, ApJ, 774, L21
 Mimica, P., Aloy, M. A., & Müller, E. 2007, A&A, 466, 93
 Mizuno, Y., Pohl, M., Niemiec, J., Zhang, B., Nishikawa, K.-I., & Hardee, P. E. 2011, ApJ, 726, 62
 Nakamura, M., & Meier, D. L. 2004, ApJ, 617, 123
 Nakamura, M., Garofalo, D., & Meier, D. L. 2010, ApJ, 721, 1783 (Paper I)
 Nakamura, M., & Asada, K. 2013, ApJ, 775, 118
 Narayan, R., Kumar, P. & Tchekhovskoy, A. 2011, MNRAS, 416, 2193
 Niemiec, J. & Ostrowski, M. 2004, ApJ, 610, 851
 Niemiec, J. & Ostrowski, M. 2006, ApJ, 641, 984
 Niemiec, J., Ostrowski, M., & Pohl, M. 2006, ApJ, 650, 1020
 Ostrowski, M., & Bednarz, J. 2002, A&A, 394, 1141
 Owen, F. N., Hardee, P. E., & Cornwell, T. J. 1989, ApJ, 340, 698
 Pelletier, G., & Pudritz, R. E. 1992, 394, 117
 Perlman, E. S., Harris, D. E., Biretta, J. A., Sparks, W. B., & Macchetto, F. D. 2003, ApJ, 599, L65
 Perlman, E. S., Biretta, J. A., Zhou, F., Sparks, W. B., & Macchetto, F. D. 1999, AJ, 117, 2185
 Perlman, E. S., & Wilson, A. S. 2005, ApJ, 627, 140
 Perlman, E. S., Adams, S. C., Cara, M., *et al.* 2011, ApJ, 743, 119
 Rieger, F. M., Bosch-Ramon, V., & Duffy, P. 2007, Astrophys. Space Sci., 309, 119
 Sanders, R. H. 1983, ApJ, 266, 73
 Schure, K. M., Bell, A. R., Drury, L. O'C., & Bykov, A. M. 2012, Space Sci. Rev., 173, 491
 Sironi, L., & Spitkovsky, A. 2009, ApJ, 698, 1523
 Sokolov, A., Marscher, A. P., & McHardy, I. M. 2004, ApJ, 613, 725
 Spada, M., Ghisellini, G., Lazzatti, D., & Celotti, A. 2001, MNRAS, 325, 1559
 Sparks, W. B., Biretta, J. A., & Macchetto, F. 1996, ApJ, 473, 254
 Spitkovsky, A. 2008, ApJ, 682, L5
 Tonry, J. L. 1991, ApJ, 373, L1
 Wang, C.-C., & Zhou, H.-Y. 2009, MNRAS, 395, 301
 Waxman, E. 1997, ApJ, 485, L5
 Wilson, A. S., & Yang, Y. 2002, ApJ, 568, 133